IET Renewable Power Generation

Special Issue Call for Papers

Be Seen. Be Cited.
Submit your work to a new IET special issue

Connect with researchers and experts in your field and share knowledge.

Be part of the latest research trends, faster.

Read more

The Institution of Engineering and Technology

Received: 25 December 2022 | Revised: 19 September 2023 | Accepted: 7 November 2023

IET Renewable Power Generation

DOI: 10.1049/rpg2.12886

The Institution of Engineering and Technology WILEY

ORIGINAL RESEARCH

Optimal gear ratio selection of linear primary permanent magnet vernier machines for wave energy applications

Reza Jafari[1] | **Pedram Asef**[2] | **Pouria Sarhadi**[1] | **Xiaoze Pei**[3]

[1]Department of Engineering and Technology, University of Hertfordshire, Hatfield, UK

[2]Department of Mechanical Engineering, University College London, London, UK

[3]Department of Electronic and Electrical Engineering, University of Bath, Bath, UK

Correspondence
Pedram Asef, Department of Mechanical Engineering, University College London, London, WC1E 7JE, UK.
Email: pedram.asef@ucl.ac.uk

Abstract

Linear permanent magnet vernier generators offer a high capability of force density, making them appealing configurations for wave energy harvesting systems. In absolute terms, the performance of these machines is significantly influenced by the selection of slot/pole combinations based on the magnetic gearing effect. For the first time, this paper aims to investigate the impact of different gear ratios on a wide array of linear primary permanent magnet vernier machines (LPPMVMs) with different slot/pole combinations based on fair criteria to offer a more comprehensive understanding of gear ratio selection. To find the optimal number of slots and poles, the response surface methodology is adopted to obtain a robust design and make a fair comparison among LPPMVMs with optimum design characteristics using a cost-effective approach for the fast and reliable optimisation process. The higher gear ratios result in higher thrust force capability. This will help establishing a new route toward faster develpment of advanced LPPMVMs. The power loss models of LPPMVMs are studied to predict their steady-state and transient thermal behaviours, verifying their stability and safety, while a simple external forced convection method can be utilised. To verify the model, finite element analysis is exploited to confirm the electromagnetic and thermal analysis results and provide a more exhaustive investigation.

1 | INTRODUCTION

Renewable energy resources have gained attraction as substitutes for fossil fuels due to their significant advantages, including being clean and free and having no adverse environmental impacts [1]. Wave energy applications are among the most significant kinds of renewable energy systems that can be exploited to transform wave motions into electrical power [2, 3]. The ocean wave industry possesses the capability to generate 300 GW by 2050, indicating the rapid progress of the wave energy industry. Also, 100 GW of generating capacity is predicted to be installed in Europe by 2050, which can meet 10% of electricity demands [4]. On the other hand, the devices to transform wave energy into electricity play a meaningful position in the development of this industry. Direct-drive linear PM vernier generators are extensively used to harvest electricity owing to their capability of providing high force density at low speeds without deploying intermediate equipment [5, 6].

Direct-drive linear permanent magnet synchronous generators (LPMSGs) are widely adopted to transform the linear motion of waves into electrical power owing to their superior advantages, such as high power density and high efficiency [7, 8]. Nevertheless, a high power density can be reached for a linear PM synchronous generator with a high number of poles [9]. Accordingly, the trend toward adopting linear generators with a high force capability has considerably augmented [10]. Linear permanent magnet vernier generators (LPMVGs) are ideal candidates to provide a high force density at low speeds. The working principles of vernier structures are established on the magnetic gearing effect similar to magnetic gears, which allows them to offer a high force density [11, 12].

A linear primary permanent magnet vernier machine (LPPMVM) was proposed in [13] and used in wave energy applications. The LPPMVM uses a long translator, and the magnets and the armature windings are located on the short stator, which makes the linear structure a robust and cost-effective option. The LPPMVM was compared with a linear vernier hybrid machine (LVHM) in [14], in which the LPPMVM offers a higher thrust force and lower cogging force. The thrust force performance of an LPPMVM was improved in [15] by

employing the spoke-type magnets and a non-magnetic space between the stator and magnets. A double-sided spoke-type linear vernier generator, used for wave energy extraction systems, was developed from a LPPMVM in [16]. Furthermore, the double-sided spoke-type linear vernier generator was equipped with high-temperature superconductor bulks in [17] to reduce the leakage flux. Even though the electromagnetic performance of linear vernier machines has been highly improved in different pieces of research, the impact of the gear ratio is required to be investigated for selecting the optimal number of slots and poles. Indeed, the combination of slots and poles in the LPPMVM is a decisive factor in the design procedure of linear vernier machines, and the logic behind the selection of gear ratio is of high essence based on the magnetic gearing effect.

The optimal number of slot/pole combinations for different rotational PM synchronous machines was studied in [18]. Nevertheless, selecting the number of slots and poles becomes more critical when vernier structures are taken into account, necessitating a more profound review. The impact of the gear ratio on the performance of eight rotational surface-mounted PM vernier machines with different slot/pole combinations was studied in [19] and established based on an analytical approach. Although the design process is accomplished in a short time, a more accurate design procedure is required to obtain a reliable comparison among vernier machines. Different PM vernier machines have been surveyed in [20] with overlap-winding and tooth-concentrated nonoverlap winding to explore the most efficient combination of slots and poles. Also, five different linear PM vernier structures were proposed in [21], employing long stators and short translators with magnets and armature windings. However, the research lacks a comprehensive investigation to study a broader range of vernier machines with various gear ratios. Additionally, the impact of the gear ratio on the performance of linear vernier machines in terms of the relationship of the magnetic gearing effect is unknown for the LPPMVM, while a more precise design procedure is also required to be accomplished in a short time.

This paper investigates the slot/pole combination of twenty different LPPMVMs employed in wave energy harvesting systems based on different criteria, such as average thrust force, thrust force density, and average force per PM volume. The design choices for linear machines in wave energy systems are analysed using the design of experiment matrices. Then, the best design is traced by exploiting the response surface methodology (RSM). The most significant contribution of this paper, which has never been achieved, is providing a comprehensive analysis of the gear ratio impact on a wider array of LPPMVMs through the exploitation of numerical analysis based on fair criteria to offer a more comprehensive insight into the selection of gear ratio and obtain a cost-effective approach for the fast and reliable optimisation process. The power loss models of LPPMVMs are also realised to predict the temperature rise based on the transient and steady-state thermal analyses. Finally, the optimised model is verified using the 2D FEA method.

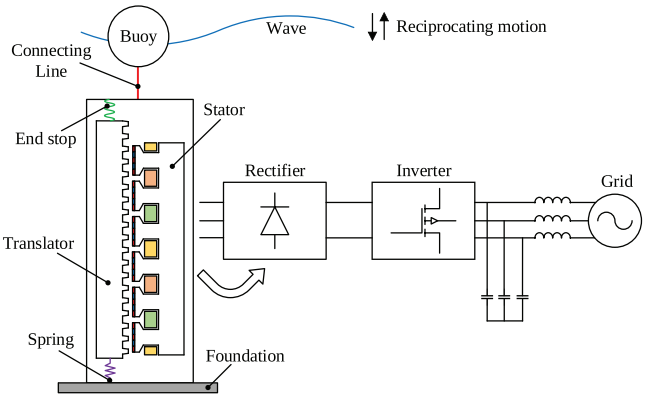

FIGURE 1 A linear primary permanent magnet vernier machine (LPPMVM) used in a wave energy harvester based on the concept of a simple point absorber converter.

2 | METHODOLOGY AND PROBLEM STATEMENT

A linear primary PM vernier machine is considered a benchmark in this paper, as shown in Figure 1, used in a wave energy harvester based on the concept of a simple point absorber converter.

The challenges associated with the exploitation of linear generators in wave energy harvesting systems can cause uncertainties in the reciprocal motion of the mover of the generator. The wave behaviours can cause fluctuations in the movement of the generator, and the environmental conditions can affect its performance. Furthermore, by conducting a robust mechanical design through the adoption of an effective modelling strategy and constructing the translator utilising suitable materials with high durability, the lifetime of the system can be extended significantly. Regular maintenance and real-time monitoring are other practical approaches to tackle the uncertainties related to the generator and its moving part [22].

Another crucial concern regarding the protection of the overall system arises during high tides and powerful waves. Accordingly, the system is required to possess the capability of withstanding harsh conditions and dissipating the excess energy to prevent it from reaching the linear generator. The system necessitates well-engineered, watertight enclosures to ward off water ingress and robust resistance to corrosion and degradation in marine environments. Predicting the periods of elevated and forceful wave activity provides the opportunity for proactive strategies, such as shutting down procedures to temporarily halt the operation of the generator under severe wave conditions [23].

The study of the performance of wave energy converters and the reliability analysis of the system are beyond the scope of this research. Nevertheless, the issues pertaining to the performance of the linear generator that affect the overall system have been taken into account in this research. The impact of optimal gear ratio selection is presented to improve electromagnetic

capability via selectable design choices. Furthermore, the operation concept of vernier structures is required to be analysed foremost, and the relationship based on the magnetic gearing effect is examined.

2.1 | Operation principles of linear primary PM vernier machines

The operation principles of LPPMVMs are the same as magnetic gears. Hence, the combination of slots and poles of linear vernier structures is defined based on the relationship of the magnetic gearing effect [24, 25]:

$$Z = P_{\mathrm{PM}} \pm P_a \tag{1}$$

where Z is the number of translator teeth, P_{PM} is the number of PM pole pairs, and P_a is the number of armature winding pole pairs. Equation (1) indicates the selection of slot/pole combinations can be obtained by employing two different relationships based on the magnetic gearing effect:

$$Z = P_{\mathrm{PM}} + P_a \tag{2}$$

$$Z = P_{\mathrm{PM}} - P_a \tag{3}$$

The gear ratio (GR) is an important criterion to define the electromagnetic performance of vernier structures, which can be expressed as the ratio of the number of PM pole pairs to the number of armature winding pole pairs.

$$\mathrm{GR} = \frac{P_{\mathrm{PM}}}{P_a} \tag{4}$$

The magnetomotive force (MMF) of a linear vernier structure can be calculated by:

$$F_{\mathrm{PM}}(t, t_t) \approx F_{\mathrm{PM1}} \cos\left(P_{\mathrm{PM}} \frac{2\pi}{L}(t - t_t)\right) \tag{5}$$

where F_{PM1} is the MMF fundamental component, t is the initial position, t_t is the translator displacement, and L is the effective length. Also, the permeance of the airgap can be expressed as follows:

$$\Lambda(t) \approx \Lambda_0 - \Lambda_1 \cos\left(Z \frac{2\pi}{L} t\right) \tag{6}$$

where Λ_0 and Λ_1 are the airgap permeance constant and fundamental components. Then, the relationship of the flux linkage can be calculated by considering some approximations:

$$\lambda_{\mathrm{ph}}(t_t) = \frac{N_{\mathrm{ph}} W}{q} \sum_{k=0}^{q-1} \int_{t_i + k\tau}^{t_i + k\tau + \frac{L}{2P_a}} B(t, t_t)\, dx$$

$$\approx 2k_{1q} N_{\mathrm{ph}} W \left(\frac{B_{\mathrm{PM0}}}{P_{\mathrm{PM}} \frac{2\pi}{L}} + \frac{B_{\mathrm{PM1}}}{2P_a \frac{2\pi}{L}}\right) \sin\left(P_{\mathrm{PM}} \frac{2\pi}{L} t_t\right) \tag{7}$$

where N_{ph} is the number of turns per phase, W is the stack length, q is the number of teeth per pole per phase, t_i is the initial position of phase winding, τ is the tooth pitch, and k_{1q} is the winding factor. Moreover, $B(t, t_t)$ is the function of the airgap flux density and is determined by the following relationship:

$$B(t, t_t) = F_{\mathrm{PM}}(t, t_t) \Lambda(t) \tag{8}$$

The back-electromotive force (EMF) of one phase (e_{ph}) can be calculated through the use of the following relationship:

$$e_{\mathrm{ph}}(t) = \frac{d\lambda_{\mathrm{ph}}(t_t)}{dt}$$

$$= 2k_{1q} N_{\mathrm{ph}} W v_m \left(B_{\mathrm{PM0}} + \frac{P_{\mathrm{PM}} B_{\mathrm{PM1}}}{2P_a}\right) \cos\left(P_{\mathrm{PM}} \frac{2\pi}{L} t_t\right) \tag{9}$$

where v_m is the velocity, B_{PM0} and B_{PM1} are the functions of the MMF fundamental and the airgap permeance components. Based on the operation principles and relationships of the linear vernier machines, the selection of the magnetic gearing effect based on (3) results in a higher thrust force. This claim is investigated in this paper by considering LPPMVMs with different slot/pole combinations. The induced voltage amplitude can be obtained as:

$$E_{\mathrm{ph}} = \sqrt{2} k_{1q} N_{\mathrm{ph}} W v_m \left(F_{\mathrm{PM1}} \left(P_0 + \frac{6q - 1}{2} P_1\right)\right) \tag{10}$$

where P_0 and P_1 are calculated by exploiting the conformal mapping method [26, 27]:

$$P_0 = \frac{\mu_0}{g}(1 - 1.6\beta c_0) \tag{11}$$

$$P_1 = \frac{2\mu_0 \beta}{g\pi} \left(\frac{0.78125}{0.78125 - 2c_0^2}\right) \sin(1.6\pi c_0) \tag{12}$$

where μ_0 is the coefficient of the vacuum permeability, c_0 is the ratio of slot width to the slot pitch, g is the distance between the tip of the stator and translator teeth, and β is Carter's coefficient. The next relationship shows how β can be calculated for linear vernier machines based on some approximations:

$$\beta = k_\beta \frac{w_s}{g} = k_\beta \frac{c_0 L}{6P_a q g} \tag{13}$$

As a result, the relationship of the induced voltage amplitude can be reformed as:

$$E_{\mathrm{ph}} = \frac{4\sqrt{2}}{\pi \mu_r} B_r k_{1q} N_{\mathrm{ph}} W v_m \frac{g_m}{g} (k_{\mathrm{conv}} + k_{\mathrm{add}}) \tag{14}$$

$$k_{\mathrm{conv}} = 1 - 1.6 k_\beta \frac{L}{6P_a q g} c_0^2 \tag{15}$$

$$k_{\mathrm{add}} = k_\beta \frac{c_0 L}{P_a g} \left(1 - \frac{1}{6q}\right) \left(\frac{0.78125}{0.78125 - 2c_0^2}\right) \sin(1.6\pi c_0) \tag{16}$$

where B_r is the residual flux of PMs, and g_m is the PM thickness. Also, the output power can be defined:

$$P_{\text{out}} = 3I_{\text{ph}}E_{\text{ph}} = k_\tau A_g v_m \frac{g_m}{g}(k_{\text{conv}} + k_{\text{add}}) \tag{17}$$

$$k_\tau = \frac{2\sqrt{2}}{\pi\mu_r} k_{1q} k_s B_r \tag{18}$$

$$k_s = \frac{6N_{\text{ph}}I_{\text{ph}}}{L} \tag{19}$$

Finally, the output power can be rewritten, and the force can be calculated as:

$$P_{\text{out}} = k_\tau A_g v_m \frac{g_m}{g}\left(1 + k_o k_\beta \frac{L}{g}\right) \tag{20}$$

$$k_o = \frac{c_0}{p}\left(1 - \frac{1}{6q}\right)\left(\frac{0.78125}{0.78125 - 2c_0^2}\right) \times sin(1.6\pi c_0) - 1.6\frac{c_0^2}{6P_a q} \tag{21}$$

$$F_{\text{out}} = k_\tau A_g \frac{g_m}{g}\left(1 + k_o k_\beta \frac{L}{g}\right) \tag{22}$$

Once the relationships governing linear vernier machines are calculated, the problem statement can be defined.

2.2 | Problem statement

Different slot/pole combinations of high force density LPPMVMs are selected in this study based on the benchmark 17-slots/18-pole pairs LPPMVM to satisfy the relationship of the magnetic gearing effect, as tabulated in Table 1. Hence, the impact of the gear ratio on the performance of LPPMVMs can be surveyed by considering a diverse combination of slots and poles.

2D schematics of two LPPMVMs are depicted in Figure 2, that is, the benchmark 17-slots/18-pole pairs LPPMVM and a 34-slots/36-pole pairs LPPMVM with the same gear ratios. The linear vernier machines employ a long secondary and a short primary equipped with magnets and armature windings. The magnets are located on the surface of the stator teeth, as shown in Figure 2 with the polarity of magnets, and three-phase single-layer distributed armature windings are adopted to achieve smoother and more sinusoidal outputs.

The procedure to study the effect of gear ratios on different LPPMVMs is shown in Figure 3. Population-based algorithms, such as genetic algorithm (GA) and particle swarm optimisation (PSO), based on finite element models of electrical machines, are known as commonly accurate optimisation methods, particularly for vernier machines owing to the ability to model the harmonic components. Nevertheless, the optimisation process requires substantial computational time and computing capability for global searching of the design spaces of different LPPMVMs. To reduce the computational burden, the response surface method (RSM) based on finite element modelling is exploited to optimise different linear vernier machines in a shorter time with high accuracy.

The process commences when 2D models of the linear vernier structures with different slot/pole combinations are established based on the 17/18 LPPMVM. A sensitivity analysis is performed based on finite element modelling to define the

TABLE 1 Different slot/pole combinations of linear primary permanent magnet vernier machines (LPPMVMs).

Model	Stator teeth	Armature winding pole pairs	PM pole pairs	PMs per stator tooth	Translator teeth	Gear ratio
01	6	1	12	3	11	12
02	6	1	15	4	14	15
03	6	1	18	5	17	18
04	6	1	21	6	20	21
05	6	1	24	7	23	24
06	12	2	24	3	22	12
07	12	2	30	4	28	15
08	12	2	36	5	34	18
09	12	2	42	6	40	21
10	12	2	48	7	46	24
11	6	1	12	3	13	12
12	6	1	15	4	16	15
13	6	1	18	5	19	18
14	6	1	21	6	22	21
15	6	1	24	7	25	24
16	12	2	24	3	26	12
17	12	2	30	4	32	15
18	12	2	36	5	38	18
19	12	2	42	6	44	21
20	12	2	48	7	50	24

Abbreviations: PM, permanent magnet.

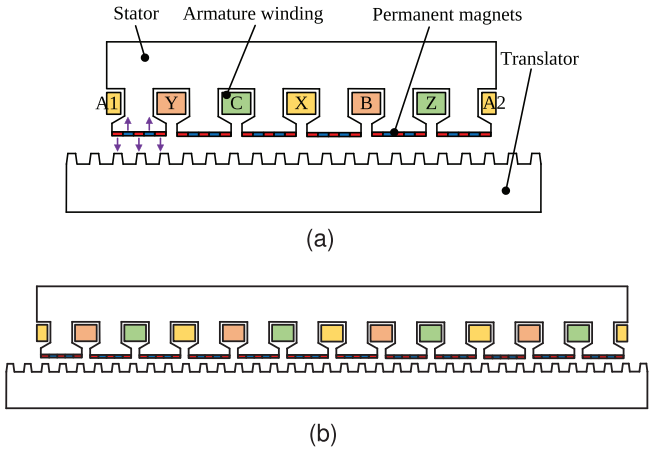

FIGURE 2 Schematic demonstration of linear primary permanent magnet vernier machines (LPPMVMs) with: (a) 17-slots/18-poles, (b) 34-slots/36-poles.

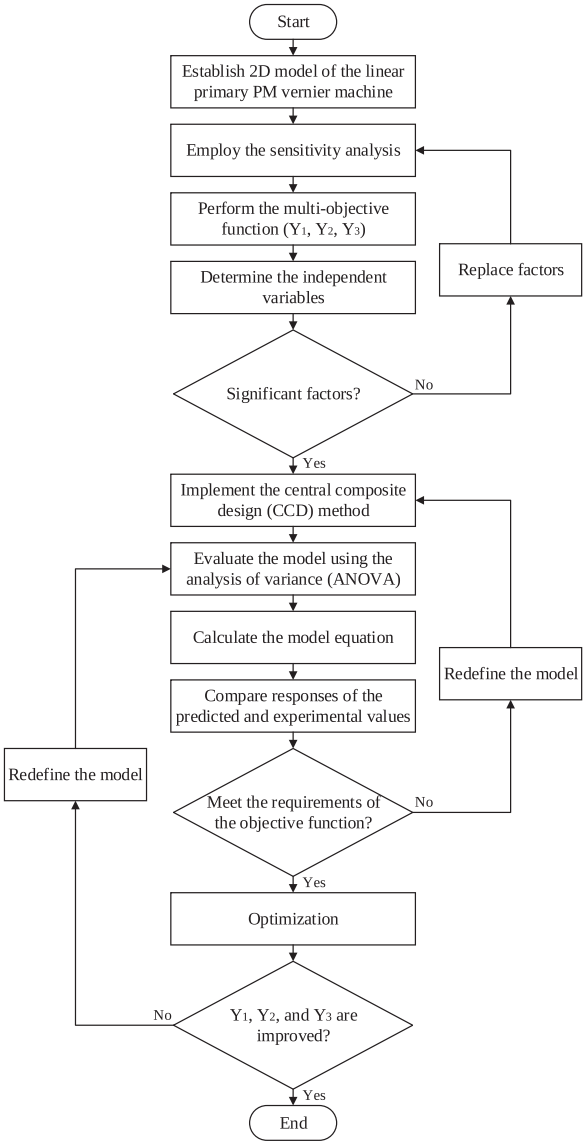

FIGURE 3 The flow chart to study the effect of gear ratio on different linear primary permanent magnet vernier machines (LPPMVMs). PM; permanent magnet.

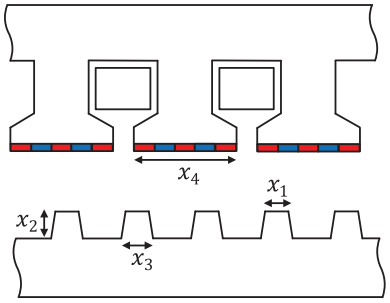

FIGURE 4 Independent variables of a linear primary permanent magnet vernier machine (LPMMVM).

TABLE 2 Design characteristics of the 17/18 linear primary permanent magnet vernier machines (LPPMVM) [13].

Item	Unit	Value
Number of phases		3
Rated frequency	Hz	50
Rated velocity	m/s	1
Airgap length	mm	1
Thickness of LPPMVM	mm	158
Stack length	mm	100
Stator tooth pitch	mm	60
Translator tooth pitch	mm	21.17
PM remanence	T	1.2
PM thickness	mm	4
Number of winding turns		142

Abbreviations: PM, permanent magnet.

significant parameters that have the most considerable impact on the performance of the machine. The Monte Carlo method is used to accomplish the sensitivity analysis, and random samples are produced by using Latin hypercube sampling (LHS). Afterwards, a multi-objective function is defined to improve the average thrust force (Y_1) and power factor (Y_2) while the thrust force ripple (Y_3) is reduced. The width of the translator tooth tip (x_1), the height of the translator tooth (x_2), and the width of the translator tooth root (x_3) are selected as the significant factors to optimise the linear machines. Moreover, the width of magnets is another significant parameter that influences the performance of the linear vernier structures, and the stator tooth width (x_4) is considered another variable to optimise the width of magnets. The parameters with the capability to be controlled and obtain a reliable prediction of the system response are depicted in Figure 4. The factors are needed to be replaced if they are insignificant. In the next step, the design of experiments can be used for the analysis of LPPMVMs.

3 | DESIGN OF EXPERIMENTS FOR LPPMVMS WITH DIFFERENT GEAR RATIOS

The performance of linear vernier machines with different combinations of slots and poles can be fairly evaluated if they are working under their optimal conditions. Accordingly, a robust optimisation procedure is required to obtain the optimal characteristics of LPPMVMs, as explained in Figure 3. The key design characteristics of the benchmark 17/18 LPPMVM have been presented in Table 2, in which different linear vernier generators are developed based on the 17/18 LPPMVM with the same stack length, the number of winding turns, the thickness of the linear machines, input current, airgap length, PM thickness, frequency, and velocity.

The response surface method can be utilised to obtain a relation between the parameters and the response. Central composite design (CCD) is employed to fit a second-order model of a response surface. This aim can be accomplished by optimising the system response (Y), in that the design objective is a

TABLE 3 Optimisation parameters and factor levels.

	Coded levels				
Independent variables	$-\alpha$	-1	**0**	$+1$	$+\alpha$
x_1	8.0	9.8	11.5	13.3	15.0
x_2	7.0	10.3	13.5	16.8	20.0
x_3	5.0	6.3	7.5	8.8	10.0
x_4	50	54	58	61	65

function of the factors (x_i):

$$Y = f(x_1, x_2, x_3, \ldots, x_n) \tag{23}$$

The Taylor series of the system response can be expressed as [28, 29]:

$$Y = \beta_0 + \sum_{i=1}^{k} \beta_i x_i + \sum_{i=1}^{k} \beta_{ii} x_i^2 + \sum_{i<j}^{k} \sum \beta_{ij} x_i x_j \tag{24}$$

$$x = \begin{bmatrix} x_1 \\ x_2 \\ \ldots \\ x_k \end{bmatrix}, b = \begin{bmatrix} \beta_1 \\ \beta_2 \\ \ldots \\ \beta_k \end{bmatrix}, B = \begin{bmatrix} \beta_{11} & \beta_{12}/2 & \ldots & \beta_{1k}/2 \\ \ldots & \beta_{22} & \ldots & \beta_{2k}/2 \\ \ldots & \ldots & \ldots & \ldots \\ sym. & \ldots & \ldots & \beta_{kk} \end{bmatrix} \tag{25}$$

where β_0, β_i, β_{ii}, and β_{ij} are the constant, linear, quadratic, and interaction coefficients, respectively. x_i and x_j are coded design variables, and k is the number of variables. x is a $k \times 1$ matrix of variables, b is a $k \times 1$ matrix of first-order regression coefficients, and B is a $k \times k$ matrix of quadratic coefficients. Afterwards, the model is evaluated using the analysis of variance (ANOVA) in order to verify the model and study the influence of significant factors. The model equation is calculated, and the responses of the predicted and experimental values are compared. Then, the process is accomplished if the requirements of the objective function are met; otherwise, the previous steps are carried out again.

The process involves thirty experiments using a central composite design matrix (CCD) coupled with a 2D-FEA tool for electromagnetic analysis of the models. By considering n as the number of factors, 2^n factorial runs and $2n$ axial runs are needed. As aforementioned, four controllable variables, including the translator tooth tip (x_1), the height of the translator tooth (x_2), the width of the translator tooth root (x_3), and the stator tooth width (x_4), are selected to optimise the linear vernier machines. Also, six centre points are required to study the experimental errors; a total of 30 runs are performed in this research. The design of experiments is carried out for LPPMVMs developed from the benchmark 17/18 LPPMVM. For example, the detailed calculations are provided only for the 20/21 LPPMVM. The coded levels for the 20/21 LPPMVM are presented in Table 3, in which ± 1, $\pm\alpha$, and 0 are applied for the factorial, axial, and centre points, respectively.

The experimental design and results of the 20/21 LPPMVM are presented in Table 4. The improvable machine parameters, such as average force, power factor, and thrust force ripple, are obtained from the FEA based on the coded levels.

The quadratic model is used for the average thrust force and the power factor, and the linear model is selected for the thrust force ripple. The response for factor levels can be predicted by adopting the coded equations. The final equations of average force (Y_1), power factor (Y_2), and force ripple (Y_3) can be expressed as follows in terms of the coded factors.

$$\begin{aligned} Y_1 &= 1764 - 135.13x_1 + 9.96x_2 - 80.54x_3 + 127.96x_4 \\ &\quad + 5.31x_1x_2 + 5.06x_1x_3 - 10.69x_1x_4 - 4.56x_2x_3 \\ &\quad - 0.3125x_2x_4 - 8.81x_3x_4 - 64.39x_1^2 - 9.14x_2^2 \\ &\quad - 27.64x_3^2 - 109.64x_4^2 \end{aligned} \tag{26}$$

$$\begin{aligned} Y_2 &= 0.25 - 0.0075x_1 + 0.0008x_2 - 0.0133x_3 + 0.0017x_4 \\ &\quad + 0.0000x_1x_2 + 0.0000x_1x_3 + 0.0000x_1x_4 + 0.0000x_2x_3 \\ &\quad + 0.0000x_2x_4 + 0.0000x_3x_4 - 0.0058x_1^2 - 0.0008x_2^2 \\ &\quad - 0.0021x_3^2 - 0.0121x_4^2 \end{aligned} \tag{27}$$

$$Y_3 = 8.92 - 0.0875x_1 + 0.5375x_2 + 0.9208x_3 + 0.9042x_4 \tag{28}$$

The analysis of variance (ANOVA) for the response surface of the average thrust force, power factor, and thrust force ripple of the 20/21 LPPMVM are tabulated in Tables 5–7, respectively.

The values of R^2 are reported as 0.9990 for Y_1, 0.9777 for Y_2, and 0.2596 for Y_3 to show the accuracy of the predicted response. Adjusted R^2 and predicted R^2 are 0.9980 and 0.9940 for Y_1, 0.95690 and 0.8716 for Y_2, 0.1412 and -0.0763 for Y_3. Adjusted R^2 can be used to measure the adjustment of the model to the experimental data, and the predicted R^2 indicates the precision of responses for new observations. The difference between the values of adjusted R^2 and predicted R^2 is less than 0.2, in which they have a reasonable agreement. Furthermore, the predicted R^2 is negative for Y_3, showing that a more reasonable prediction of the response can be performed by using the overall mean. The ratio of signal to noise is known as adequate precision, which is desired to be greater than 4 to show the capability of the model to be exploited for design space navigation. The adequate precision values of Y_1, Y_2, and Y_3 are 123.19, 25.09, and 5.17, respectively, to indicate the ratio of the signal to noise. The standard deviation is obtained from the fit statistics, which are 9.88 for Y_1, 0.0039 for Y_2, and 2.32 for Y_3. By calculating the standard deviation and mean, the coefficient of variation (CV) can be achieved, which is 0.16% for Y_1, 1.69% for Y_2, and 25.97% for Y_3. The values of CV for Y_1 and Y_2 are very good, but Y_3 has an acceptable value of CV. The F-value equals 1021.05 for the model of average force and 46.99 for the model of power factor. However, the model F-value is 2.19 for the thrust force ripple; thus, there is a 9.91% chance that an F-value this high could occur due to noise. Also, P-values less than 0.0500 are representative of significant model terms, and P-values greater than 0.1000 show the model terms are not sig-

TABLE 4 The experimental design and results of the 20/21 linear primary permanent magnet vernier machines (LPPMVM).

		Coded levels				Finite element analysis responses		
Run	Space type	x_1	x_2	x_3	x_4	Average force [*N*]	Power factor	Thrust force ripple [%]
1	Factorial	9.8	10.3	6.8	54	1611	0.25	9.4
2	Factorial	13.3	10.3	6.8	54	1347	0.23	8.3
3	Factorial	9.8	16.8	6.8	54	1627	0.25	10.5
4	Factorial	13.3	16.8	6.8	54	1379	0.23	8.3
5	Factorial	9.8	10.3	10.3	54	1471	0.22	7.3
6	Factorial	13.3	10.3	10.3	54	1224	0.21	11.0
7	Factorial	9.8	16.8	10.3	54	1467	0.22	9.6
8	Factorial	13.3	16.8	10.3	54	1241	0.21	11.1
9	Factorial	9.8	10.3	6.8	61	1917	0.25	9.4
10	Factorial	13.3	10.3	6.8	61	1606	0.24	10.6
11	Factorial	9.8	16.8	6.8	61	1929	0.25	10.5
12	Factorial	13.3	16.8	6.8	61	1641	0.24	11.2
13	Factorial	9.8	10.3	10.3	61	1741	0.23	9.5
14	Factorial	13.3	10.3	10.3	61	1450	0.21	14.7
15	Factorial	9.8	16.8	10.3	61	1733	0.23	13.0
16	Factorial	13.3	16.8	10.3	61	1467	0.21	13.3
17	Axial	8	13.5	8.5	58	1782	0.24	10.3
18	Axial	15	13.5	8.5	58	1231	0.21	4.6
19	Axial	11.5	7	8.5	58	1697	0.24	6.3
20	Axial	11.5	20	8.5	58	1758	0.25	9.1
21	Axial	11.5	13.5	5	58	1821	0.27	5.2
22	Axial	11.5	13.5	12	58	1486	0.21	10.6
23	Axial	11.5	13.5	8.5	50	1087	0.20	5.6
24	Axial	11.5	13.5	8.5	65	1564	0.20	8.1
25	Center	11.5	13.5	8.5	58	1764	0.25	6.7
26	Center	11.5	13.5	8.5	58	1764	0.25	6.7
27	Center	11.5	13.5	8.5	58	1764	0.25	6.7
28	Center	11.5	13.5	8.5	58	1764	0.25	6.7
29	Center	11.5	13.5	8.5	58	1764	0.25	6.7
30	Center	11.5	13.5	8.5	58	1764	0.25	6.7

nificant. Thus, x_1, x_2, x_3, x_4, x_1x_2, x_1x_4, x_3x_4, x_1^2, x_2^2, x_3^2, and x_4^2 are significant model terms for the average force, and x_1, x_3, x_1^2, x_3^2, and x_4^2 are significant model terms for the power factor.

Considering the multi-objective function, the response surface optimisation is performed for the average thrust force and the power factor, as demonstrated in Figures 5 and 6 to study the impact of different factors.

Figure 5a depicts the impact of variables x_1 and x_2 on the average thrust force of 20/21 LPPMVM. As can be seen, the increase of x_1 from 9.8 to 13.3 mm and decrease of x_2 from 16.8 to 10.3 mm lead to the higher average thrust force. Also, Figure 5b,c shows the effect of x_3 versus x_1 and x_1 versus x_4 on the average force, respectively. The maximum value of average thrust force is 1830 N when x_2 and x_3 are varied. Moreover, the trend of changing x_2 versus x_4 and x_3 versus x_4 results in the highest average thrust force at 1803 and 1868 N, respectively. The figures confirm the significance of the controllable variables in calculating the optimal values. The same surface plots for the power factor are demonstrated in Figure 6, and the effect of changing variables can be observed.

4 | FINITE ELEMENT ANALYSIS OF LPPMVMs WITH DIFFERENT SLOT/POLE COMBINATIONS

The selection of the slot/pole combination is one of the most significant and influential steps during the design of lin-

TABLE 5 The analysis of variance (ANOVA) for the response surface of the average thrust force.

Source	Sum of squares	Degree of freedom	Mean square	*F*-value	*P*-value	Remarks
Model	1.396×10^6	14	99,694.31	1021.05	<0.0001	significant
x_1	4.382×10^5	1	4.382×10^5	4488.07	<0.0001	
x_2	2380.04	1	2380.04	24.38	0.0002	
x_3	1.557×10^5	1	1.557×10^5	1594.52	<0.0001	
x_4	3.930×10^5	1	3.930×10^5	4024.63	<0.0001	
x_1x_2	451.56	1	451.56	4.62	0.0482	
x_1x_3	410.06	1	410.06	4.20	0.0583	
x_1x_4	1827.56	1	1827.56	18.72	0.0006	
x_2x_3	333.06	1	333.06	3.41	0.0846	
x_2x_4	1.56	1	1.56	0.0160	0.9010	
x_3x_4	1242.56	1	1242.56	12.73	0.0028	
x_1^2	1.137×10^5	1	1.137×10^5	1164.54	<0.0001	
x_2^2	2289.07	1	2289.07	23.44	0.0002	
x_3^2	20947.65	1	20947.65	214.54	<0.0001	
x_4^2	3.297×10^5	1	3.297×10^5	3376.62	<0.0001	
Residual	1464.58	15	97.64			
Lack of fit	1464.58	10	146.46			
Pure error	0.0000	5	0.0000			
Correlation total	1.397×10^6	29				

TABLE 6 The analysis of variance (ANOVA) for the response surface of the power factor.

Source	Sum of squares	Degree of freedom	Mean square	*F*-value	*P*-value	Remarks
Model	0.0102	14	0.0007	46.99	<0.0001	Significant
x_1	0.0014	1	0.0014	86.79	<0.0001	
x_2	0.0000	1	0.0000	1.07	0.3170	
x_3	0.0043	1	0.0043	274.29	<0.0001	
x_4	0.0001	1	0.0001	4.29	0.561	
x_1x_2	0.0000	1	0.0000	0.0000	1.0000	
x_1x_3	0.0000	1	0.0000	0.0000	1.0000	
x_1x_4	0.0000	1	0.0000	0.0000	1.0000	
x_2x_3	0.0000	1	0.0000	0.0000	1.0000	
x_2x_4	0.0000	1	0.0000	0.0000	1.0000	
x_3x_4	0.0000	1	0.0000	0.0000	1.0000	
x_1^2	0.0009	1	0.0009	60.00	<0.0001	
x_2^2	0.0000	1	0.0000	1.22	0.2859	
x_3^2	0.0001	1	0.0001	7.65	0.0144	
x_4^2	0.0040	1	0.0040	257.45	<0.0001	
Residual	0.0002	15	0.0000			
Lack of fit	0.0002	10	0.0000			
Pure error	0.0000	5	0.0000			
Correlation total	0.0105	29				

TABLE 7 The analysis of variance (ANOVA) for the response surface of the thrust force ripple.

Source	Sum of squares	Degree of freedom	Mean square	*F*-value	*P*-value	Remarks
Model	47.09	4	11.77	2.19	0.0991	Significant
x_1	0.1837	1	0.1837	0.0342	0.8548	
x_2	6.93	1	6.93	1.29	0.2667	
x_3	20.35	1	20.35	3.79	0.0629	
x_4	19.62	1	19.62	3.65	0.0675	
Residual	134.29	25	5.37			
Lack of fit	134.29	20	6.71			
Pure error	0.0000	5	0.0000			
Correlation total	181.37	29				

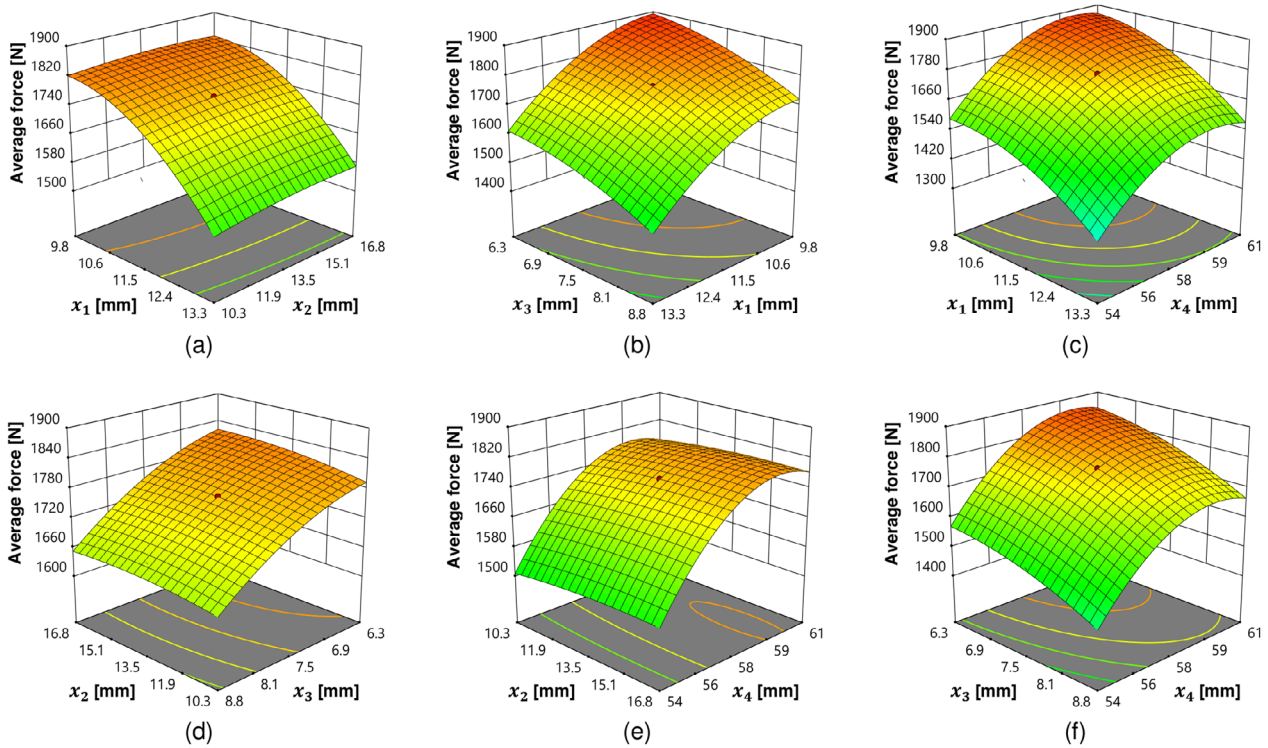

FIGURE 5 Surface plots for the average thrust force of the 20/21 linear primary permanent magnet vernier machine (LPPMVM): (a) x_1 versus x_2, (b) x_3 versus x_1, (c) x_1 versus x_4, (d) x_2 versus x_3, (e) x_2 versus x_4, and (f) x_3 versus x_4.

ear vernier machines. 2D finite element analysis is adopted to analyse the LPPMVMs with different gear ratios and make a comparison based on the impact of the combination of slots and poles on the electromagnetic behaviour of vernier machines. The magnetic flux distribution of the 17/18 LPPMVM is depicted in Figure 7, obtained from the FEA results under the no-load condition.

The experimental design and results of LPPMVMs with different slot/pole combinations are shown in Table 8, in which there are acceptable agreements between the predicted and FEA results. The predicted values of average thrust force deviate 3.21% from the FEA results for the 50/48 LPPMVM as the worst case, while the same value is reported under 2% for other configurations. The maximum difference between predicted and FEA values of power factor is 0.1, and 4.3% for the thrust force ripple. The predicted values of average force, power factor, and thrust force ripple are 1886% , 0.26% , and 7.6% for the 20/21 LPPMVM, respectively. The results achieved from the FEA have a slight deviation from the predicted values, in such a way that the difference for the average force is 0.1%, and there is no difference between power factor values. Also, the difference between predicted and FEA results of the thrust force ripple is 1.3%. Consequently, the solutions are selected for further investigation of LPPMVMs.

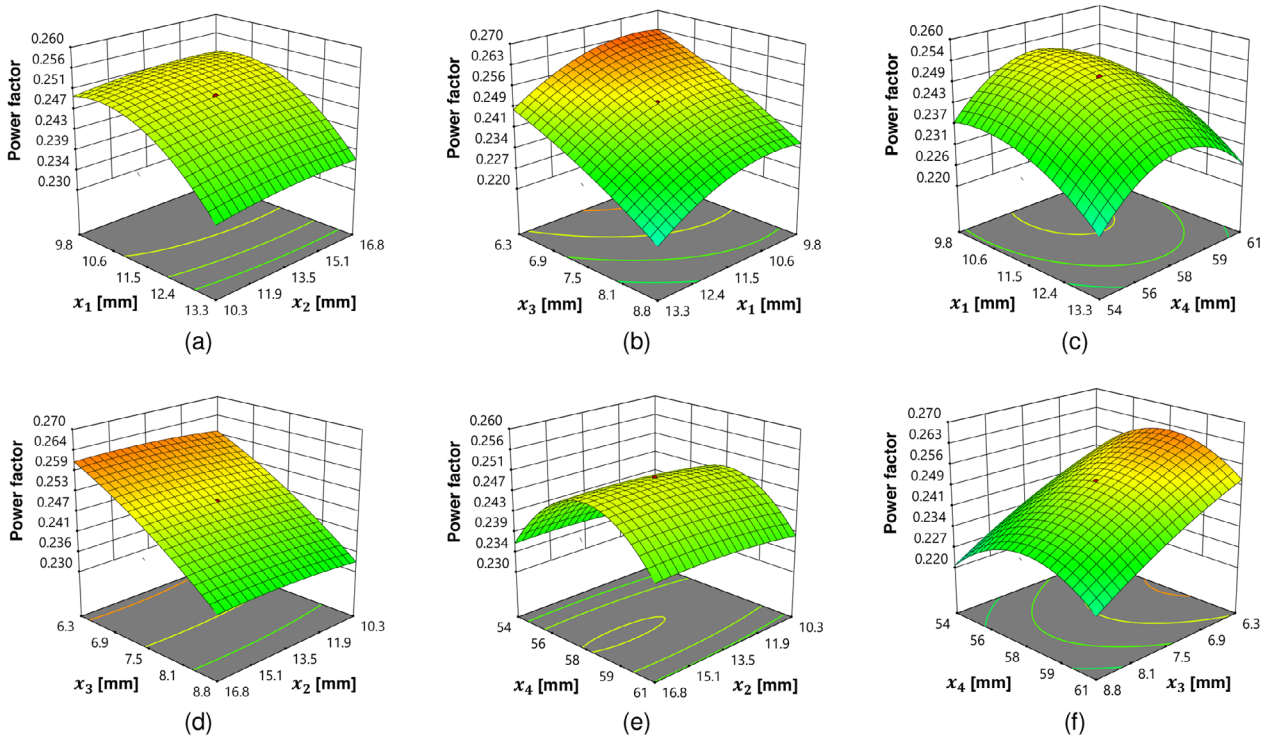

FIGURE 6 Surface plots for the power factor of the 20/21 linear primary permanent magnet vernier machine (LPPMVM): (a) x_1 versus x_2, (b) x_3 versus x_1, (c) x_1 versus x_4, (d) x_3 versus x_2, (e) x_4 versus x_2, and (f) x_4 versus x_3.

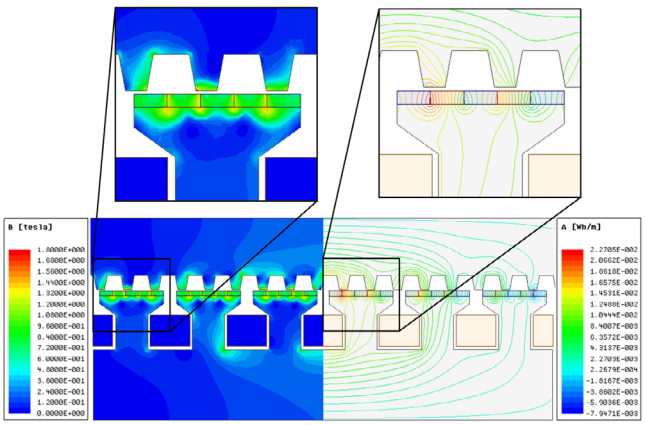

FIGURE 7 Magnetic flux (B) distribution of the 17/18 linear primary permanent magnet vernier machine (LPPMVM).

The no-load back EMF waveforms and their maximum values for phase A of LPPMVMs with different gear ratios are illustrated in Figures 8 and 9, respectively. LPPMVMs with higher gear ratios offer higher values of no-load back EMF, leading to higher force/power density values. The 17/18 LPPMVM has a maximum back-EMF amplitude of 60 V under the no-load condition. The highest value is reported at 162.5 V for the 46/48 LPPMVM, while the minimum value is reported at 32.6 V for the 11/12 LPPMVM.

Figure 10 depicts the thrust force waveforms of linear primary PM vernier generators with different gear ratios. As can be seen, the highest values of thrust force are reported for LPPMVMs with high gear ratios. The 46/48 LPPMVM has an average thrust force of 4217 N, reported as the maximum value. On the other hand, the 11/12 LPPMVM has the minimum average force of 889 N. However, LPPMVMs with different gear ratios are affected by the machine length and the optimum volume of magnets; thus, a reliable comparison can be accomplished by considering the machine dimensions and PM volume into account.

To accomplish a reasonable comparison, average thrust force per PM volume and thrust force density are compared for linear vernier generators with different slot/pole combinations. Thrust force density values for LPPMVMs with different gear ratios are depicted in Figure 11. Overall, the force density increases with higher gear ratios. However, the optimal values are required to be obtained based on a robust design of linear vernier machines. Thrust force density values for LPPMVMs with slot/pole combinations based on (2) and (3) are shown in Figure 11. The most significant point that stands out is the higher values of thrust force density that can be realised when the number of slots and poles is selected based on (3), which confirms the conclusion drawn from the operation principles of linear vernier machines. The conventional 17/18 LPPMVMV has a thrust force density of 283.0 kN/m^3, which is 6.7% higher than the 19/18 LPPMVMV counterpart with a thrust force density of 265.2 kN/m^3. The 34/36 LPPMVMV also has the same trend as the 38/36 LPPMVMV, in which trend of higher geathe former LPPMVM shows a higher thrust force density of 9.5 kN/m^3 compared to the latter one. The LPPMVMs with 11-slots/12-pole pairs, 14-slots/15-pole

TABLE 8 The experimental design and results of linear PM vernier generators with different gear ratios.

	Solutions				Average force [N]		Power factor		Thrust force ripple	
LPPMVM	x_1	x_2	x_3	x_4	**Predicted**	**FEA**	**Predicted**	**FEA**	**Predicted**	**FEA**
11/12/1	10.6	16.7	6.2	28	889	893	0.20	0.20	7.3	7.2
14/15/1	11.0	16.7	6.5	38	1265	1257	0.23	0.24	7.7	6.4
20/21/1	10.0	10.2	6.2	58	1886	1884	0.26	0.26	7.6	6.4
23/24/1	10.6	10.2	6.2	68	2098	2111	0.27	0.27	9.5	6.8
22/24/2	12.6	16.7	6.2	28	1802	1771	0.22	0.23	6.7	5.3
28/30/2	10.9	14	6.2	38	2528	2502	0.25	0.26	7.6	6.7
34/36/2	10.6	16.7	6.2	49	3161	3099	0.28	0.28	5.3	3.3
40/42/2	10.6	13.7	6.2	56	3564	3548	0.27	0.28	7.4	5.7
46/48/2	9.7	11.6	6.2	69	4217	4227	0.27	0.27	5.9	7.2
13/12/1	11.2	12.4	6.2	32	924	938	0.21	0.22	3.9	3.6
16/15/1	11.2	16.7	6.2	42	1303	1280	0.24	0.24	6.3	10.6
19/18/1	11.2	11.8	6.2	52	1558	1584	0.25	0.26	6.0	4.4
22/21/1	11.2	13.2	6.2	59	1870	1885	0.27	0.28	9.2	9.8
25/24/1	11.2	10.2	6.2	69	2086	2107	0.27	0.28	8.8	11.2
26/24/2	11.2	12.8	6.2	33	1911	1907	0.23	0.23	2.1	2.4
32/30/2	11.3	16.6	6.3	43	2547	2544	0.25	0.25	5.9	9.2
38/36/2	11.2	12.2	6.2	53	3147	3141	0.26	0.26	3.0	2.8
44/42/2	11.2	13.9	6.2	60	3891	3936	0.28	0.28	7.7	9.1
50/48/2	12.7	15.0	6.2	70	4200	4335	0.28	0.29	9.4	9.4

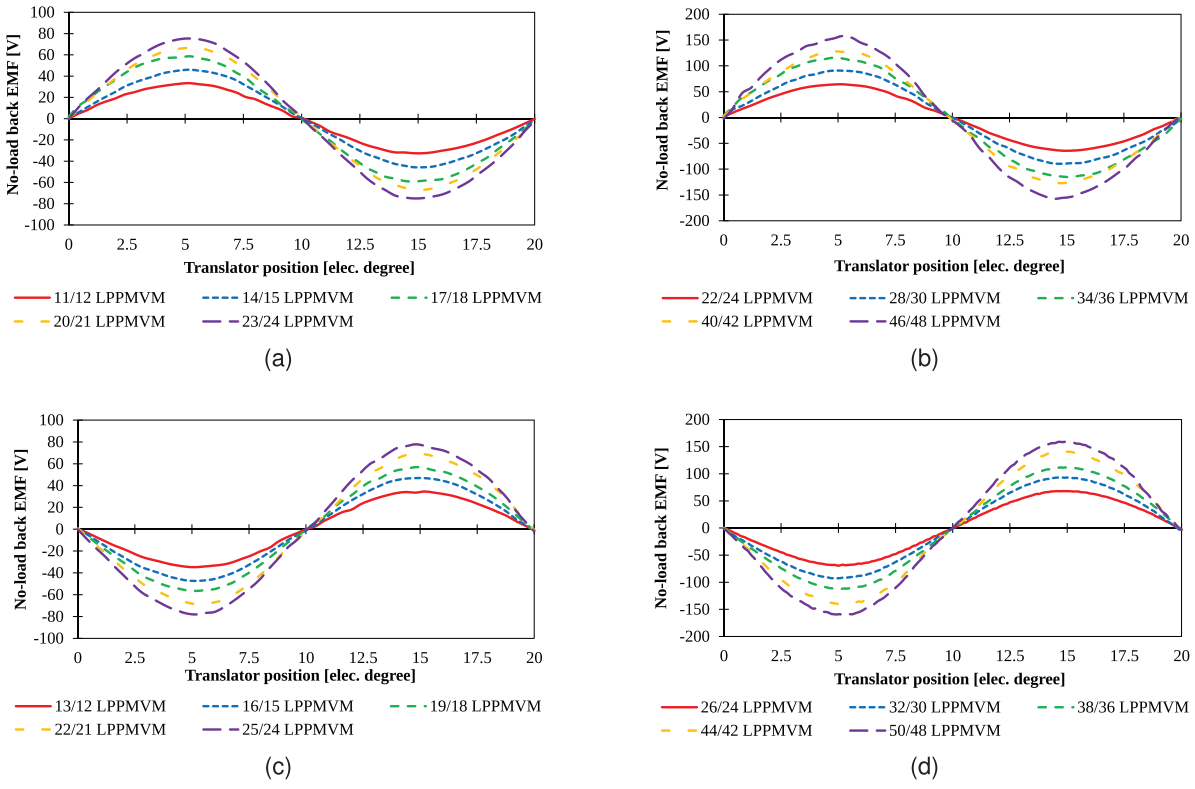

FIGURE 8 No-load back EMF waveforms of linear primary permanent magnet vernier machines (LPPMVMs) with different gear ratios: (a) LPPMVMs based on (3) with 1 armature winding pole pairs, (b) LPPMVMs based on (2) with 1 armature winding pole pairs, (c) LPPMVMs based on (3) with 2 armature winding pole pairs, (d) LPPMVMs based on (2) with 2 armature winding pole pairs. EMF; electromotive force.

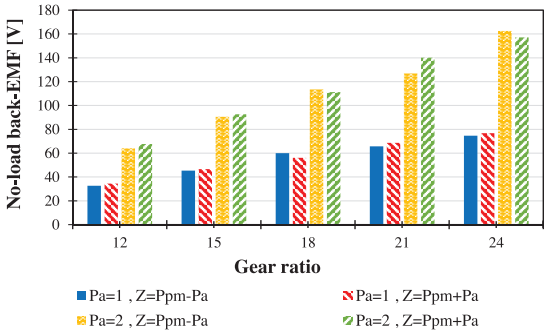

FIGURE 9 Maximum amplitude of no-load back EMF for linear primary permanent magnet vernier machines (LPPMVMs) with different gear ratios based on the magnetic gearing relationship. EMF; electromotive force.

pairs, 20-slots/21-pole pairs, and 23-slots/24-pole pairs indicate higher thrust force density values of 10.6%, 10.7%, 8.9%, and 8.0% compared to LPPMVMs with 13-slots/12-pole pairs, 16-slots/15-pole pairs, 22-slots/21-pole pairs, and 25-slots/24-pole pairs, respectively. Accordingly, the slot/pole combination of the LPPMVMs is selected based on (3) to obtain higher thrust force capabilities.

The maximum thrust force density is reported to be 296.6 kN/m^3 for the 20/21 LPPMVM, which is 4.6% higher than the 17/18 LPPMVM. On the other hand, the 13/12 LPPMVM possesses the minimum thrust force density of 230.1 kN/m^3. The higher the gear ratios, the higher values of the average force is expected. Nevertheless, the trend of higher gear ratios does not align with higher thrust force density values in some cases. By considering the magnetic gearing relationship based on (3) and 1 armature winding pole pairs, the higher gear ratios offer higher force capabilities, excluding the LPPMVMs with 23-slots/24-pole pairs and 34-slots/36-pole pairs. Moreover, the increment of gear ratios for LPPMVM with slot/pole combinations based on (2) and 1 armature winding pole pairs shows the same behaviour excluding the 25/24 and 50/48 LPPMVMs. LPMVMs with different gear ratios undergo an optimisation process, and their most optimum performance is achieved. The ratio of the average thrust force to the machine volume is the criterion to depict the impact of the optimality of LPMVMs. Upon closer examination, some structures with higher gear ratios might offer lower thrust force density values. The behaviour arises from the poor capability of these linear machines to exploit the maximum utilisation of magnets and volumes of these structures. Nevertheless, the general trend shows that high gear ratios lead to higher values of thrust force density. This necessitates adopting a practical optimisation process to select the most beneficial structure and achieve the maximum force density.

To enrich the investigation on the impact of gear ratios on the force performance of linear vernier generators, the average thrust force per PM volume of LPPMVMs is also calculated. The maximum average thrust force is 4335 N for the LPPMVM with 50-slots/48-pole pairs owing to the high amount of magnets and higher dimensions of the linear structure. However, the thrust force per PM volume equals 12.9 N/cm^3,

TABLE 9 Thrust force density and average thrust force per permanent magnet (PM) volume for linear primary permanent magnet vernier machines (LPPMVMs) with different slot/pole combinations.

LPPMVM [slot/pole]	PM volume [cm^3]	Force density [kN/m^3]	Force per PM volume [N/cm^3]
11/12/1	67.2	254.5	13.2
14/15/1	91.2	282.1	13.7
17/18/1	120.0	283.0	13.4
20/21/1	139.2	296.6	13.5
23/24/1	163.2	289.2	12.9
22/24/2	134.4	252.4	13.1
28/30/2	182.4	280.7	13.7
34/36/2	235.2	272.4	13.1
40/42/2	268.8	283.5	13.2
46/48/2	331.2	293.3	13.7
13/12/1	76.8	230.1	12.7
16/15/1	100.8	254.7	12.7
19/18/1	124.8	265.2	12.7
22/21/1	141.6	272.3	13.3
25/24/1	165.6	267.7	12.7
26/24/2	158.4	233.9	12.0
32/30/2	206.4	253.1	12.3
38/36/2	254.4	262.9	12.3
44/42/2	288.0	284.3	13.6
50/48/2	336.0	275.4	12.9

which highlights the poor utilisation of magnets among other LPPMVMs with different slot/pole combinations. Due to the high price of permanent magnets, particularly neodymium iron boron (NdFeB) magnets, average force per PM volume values of LPPMVMs are required to be compared. The 17/18 LPPMVM has a force per PM volume of 13.4 N/cm^3, which is 2.1% less than the 14/15 LPPMVM and 0.7% less than the 20/21 LPPMVM. However, the same criteria for the 17/18 LPPMVM compared to the counterpart 19/18 LPPMVM are improved by 5.5%. Although all linear vernier structures show a higher average force per PM volume compared to their linear PM synchronous counterparts, the PM volume is needed to be optimised. The detailed values of thrust force density and average thrust force per PM volume for LPPMVMs with different slot/pole combinations are summarised in Table 9.

The thrust force ripple of LPPMVMs is calculated based on the following relationship

$$F_{\text{ripple}} = \frac{F_{\max} - F_{\min}}{F_{\text{avg}}} \tag{29}$$

where $F_{\max}$ is the maximum value of thrust force, $F_{\min}$ is the minimum value of thrust force, and F_{avg} is the average value of thrust force. The 17/18 LPPMVM has a low thrust force ripple of 3.1%, which is regarded as an impressive advantage for

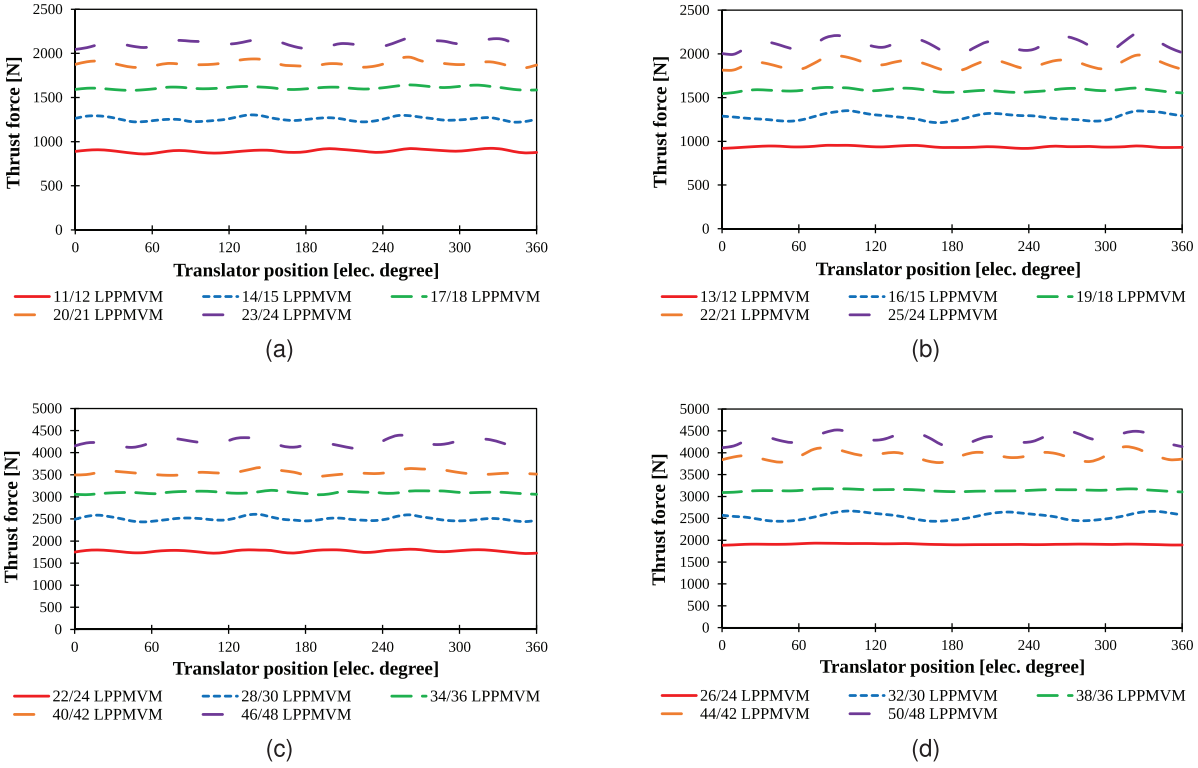

FIGURE 10 Thrust force waveforms of linear primary permanent magnet vernier machines (LPPMVMs) with different gear ratios: (a) LPPMVMs based on (3) with 1 armature winding pole pairs, (b) LPPMVMs based on (2) with 1 armature winding pole pairs, (c) LPPMVMs based on (3) with 2 armature winding pole pairs, (d) LPPMVMs based on (2) with 2 armature winding pole pairs.

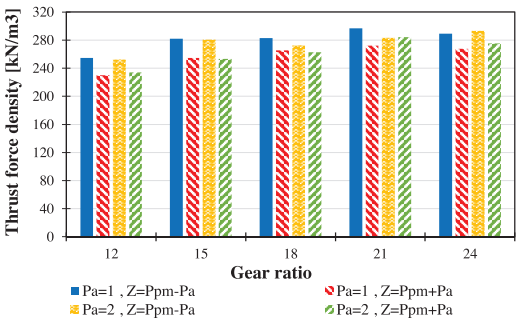

FIGURE 11 Thrust force density for linear primary permanent magnet vernier machines (LPPMVMs) with different gear ratios based on the magnetic gearing relationship.

applications requiring a smooth operation of the linear vernier machine. Also, the 26/24 LPPMVM has the least value of thrust force ripple of 2.4%. The 25/24 LPPMVM suffers from the maximum thrust force ripple of 11.2%, which restricts the operation of the linear generator in addition to having lower thrust force density and thrust force per PM volume values compared to other structures. Even though the 20/21 LPPMVM has a higher thrust force ripple of 6.4% in comparison with the 17/18 LPPMVM and the 26/24 LPPMVM, its high thrust force density places the linear vernier generator with 20 slots, 21 PM pole pairs, and 1 armature winding pole pairs among the beneficial configurations of LPPMVMs.

The most undesirable feature of vernier structures is their low power factor, which arises from the principles of the magnetic gearing effect. The power factor values of LPPMVMs vary between 0.20 and 0.29, which necessitates a robust design and optimisation process for linear vernier generators. The power factor values of the proposed LPPMVMs in this paper do not follow a specific trend, and the LPPMVMs with optimal power factor values are selected based on the design requirements and the volume of magnets. Even though the 17/18 and 20/21 LPPMVMs have a power factor of 0.26, their high force density values make them appropriate structures for wave energy applications. Accordingly, LPPMVMs with 17-slots/18-pole pairs and 20-slots/21-pole pairs are reported as more practical choices by considering the requirements of wave energy systems, as bolded in Table 9.

5 | THERMAL ANALYSIS OF LPPMVMs WITH DIFFERENT SLOT/POLE COMBINATIONS

Exceeding the maximum allowable temperature can cause irreparable damages to linear PM vernier machines; particularly, the windings are vulnerable to overheating, and PMs are in danger of demagnetization. For safety and reliable operation in wave energy systems, predicting the temperature rise is regarded as an essential step in the design process of linear machines. Power loss models are required to be established; hence, the

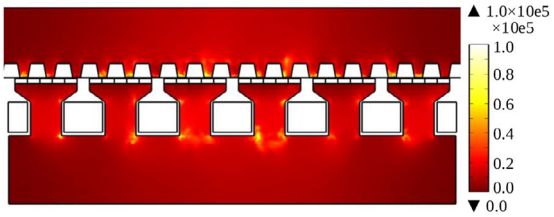

FIGURE 12 Volumetric loss density [W/m3] of 17/18 linear primary permanent magnet vernier machine (LPPMVM).

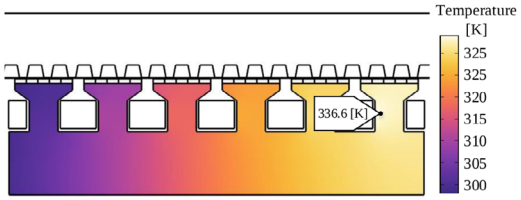

FIGURE 13 Steady-state thermal analysis of 17/18 linear primary permanent magnet vernier machine (LPPMVM).

thermal investigation can be obtained. The core and copper losses are modelled in this research as the heat sources in the thermal investigation.

The copper loss model is calculated from the resistive heating, and the equation can be expressed as:

$$P_{\text{copper}} = \frac{1}{T}\int_{T_{\text{end}}}^{T_{\text{end}}-T} J.Edt \tag{30}$$

where T is the electrical period, T_{end} is the end time, J is the current density, and E is the electric field. The copper losses are 243.5 W for LPPMVMs with 1 armature winding pole pair, and 487.1 W for LPPMVMs with 2 armature winding pole pairs. The Bertotti loss model is exploited in this paper to define core losses in LPPMVMs, including hysteresis losses, eddy current losses, and excess losses based on accurate calculations. The Bertotti loss model can be expressed as

$$P_{fe} = k_h f B_{\text{gmax}}^{b} + k_c f^2 B_{\text{gmax}}^{2} + k_e f^{1.5} B_{\text{gmax}}^{1.5} \tag{31}$$

where k_c is the eddy current loss coefficient and k_e is the excess loss coefficient [5].

The linear vernier machines are selected based on (3), due to their superiority of high thrust force density, to calculate their losses and analyse the thermal analyses. The core loss values of linear primary PM vernier structures are 20.7, 32.1, 44.4, 52.2, and 63.4 W for 11/12, 14/15, 17/18, 20/21, and 23/24 LPPMVMs, respectively. As expected, the higher gear ratios and average force values result in higher core losses. Also, core loss values for 22/24 LPPMVM is 48.2 W, 28/30 LPPMVM is 60.9 W, 34/36 LPPMVM is 82.7 W, 40/42 LPPMVM is 103.0 W, and 46/48 LPPMVM is 131.7 W. The volumetric loss density of 17/18 LPPMVMV can be seen in Figure 12.

Once the power loss values are calculated, the heat transfer mechanisms can be defined for the thermal study. Convective and conductive mechanisms are used to achieve accurate thermal models. The reference temperature is 293.15 K, and the air is considered fluid at the absolute pressure of 1 atm and a speed of 1 m/s. The steady-state thermal analysis of 17/18 LPPMVM is presented in Figure 13 under the external forced convection. The temperature of the hottest spot on the stator surface is 336.6 K, which shows the temperature rise cannot harm the vulnerable parts of the linear machine.

Moreover, the transient average temperature rise of the stator surface for other LPPMVMs is depicted in Figure 14 during 6 h of simulation. Obviously, 11/12 LPPMVM undergoes the minimum temperature rise due to the lowest losses. The temperature of 46/48 LPPMVM reaches 358.4 K at the end of the simulation. The thermal analyses of LPPMVMs with different gear ratios confirm the stability and safety of their operation, in which the undesired effects of overheating are prevented. Remarkably, the thermal analysis guarantees the

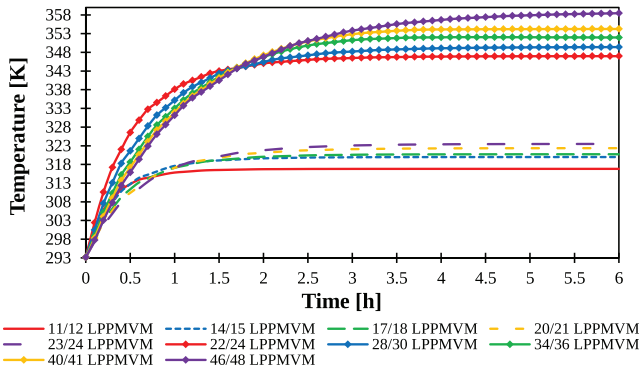

FIGURE 14 The transient average temperature rise of the stator surface of linear primary permanent magnet vernier machines (LPPMVMs).

stability and safety of 17/18 and 20/21 LPPMVMs used in wave energy harvesting systems.

6 | CONCLUSION

LPPMVMs are extensively utilised in wave energy harvesting systems due to their capability to offer a high thrust force at low speeds. Linear vernier structures function based on the same principles as magnetic gears, and the selection of their slot/pole combinations is regarded as an influential factor in defining their operational performance during their design procedure. However, further research is required to investigate the impact of the number of poles and slots on the performance of LPPMVMs. In this paper, twenty different configurations of LPPMVMs with different gear ratios are studied and compared to understand the impact of the magnetic gearing relationship for a wide range of structures. The response surface method is used in this paper to analyse the parameters change and obtain high average force and power factor values while the thrust force ripple is decreased. The responses and the predicted values are compared, and the finite element analysis is provided to model different LPPMVMs. In absolute terms, using the robust magnetic gear ratio selection based on the proposed design optimisation criteria has offered a remarkable reduction in the computation time and burden of design and optimisation processes while the accuracy is guaranteed. Higher gear ratios lead to increased back-EMF values, while the optimisation of linear machines is needed to achieve their maximum attainable thrust force density values. Furthermore, the slot/pole combination of the linear vernier structures is recommended to be selected based on $Z = P_{\mathrm{PM}} - P_a$ to obtain higher force density values. LPPMVMs are compared based on their force density and average force per PM volume to provide more exhaustive research. The transient and steady-state thermal analyses are studied based on the accurate loss model of LPPMVMs, which confirms a safe operation is yielded by adopting external forced convection. The electromagnetic and thermal results are confirmed by exploiting two-dimensional finite element analysis (2D-FEA).

AUTHOR CONTRIBUTIONS

Reza Jafari: Conceptualization; data curation; formal analysis; funding acquisition; investigation; methodology; project administration; resources; software; validation; visualization; writing — original draft. **Pedram Asef**: Conceptualization; data curation; formal analysis; funding acquisition; investigation; methodology; project administration; resources; software; supervision; validation; visualization; writing — original draft; writing — review and editing. **Pouria Sarhadi**: Conceptualization; data curation; investigation; methodology; project administration; resources; supervision; validation; visualization; writing — review and editing. **Xiaoze Pei**: Funding acquisition; methodology; project administration; supervision; validation; writing — review and editing.

CONFLICT OF INTEREST STATEMENT

The authors declare no conflicts of interest.

DATA AVAILABILITY STATEMENT

The data that support the findings of this study are available from the corresponding author upon reasonable request.

ORCID

Pedram Asef https://orcid.org/0000-0003-3264-7303

REFERENCES

1. Derakhshani, M. M., Ardebili, M., Jafari, R.: A survey on a novel double-rotor spoke-type permanent magnet induction generator employing bridged and bridgeless structures. Electr. Eng. 104(2), 899–911 (2022)
2. Wahyudie, A., Jama, M., Susilo, T.B., Mon, B.F., Shaaref, H., Noura, H.: Design and testing of a laboratory scale test rig for wave energy converters using a double-sided permanent magnet linear generator. IET Renewable Power Gener. 11(7), 922–930 (2017)
3. Khatri, P., Wang, X.: Comprehensive review of a linear electrical generator for ocean wave energy conversion. IET Renewable Power Gener. 14(6), 949–958 (2020)
4. Ahamed, R., McKee, K., Howard, I.: Advancements of wave energy converters based on power take off (PTO) systems: A review. Ocean Eng. 204, 107248 (2020)
5. Jafari, R., Asef, P., Ardebili, M., Derakhshani, M.M.: Linear permanent magnet vernier generators for wave energy applications: Analysis, challenges, and opportunities. Sustainability 14(17), 10912 (2022)
6. Derakhshani, M.M., Ardebili, M., Cheraghi, M., Jafari, R.: Investigation of structure and performance of a permanent magnet vernier induction generator for use in double-turbine wind systems in urban areas. IET Renewable Power Gener. 14(19), 4169–4178 (2020)
7. Huang, L., Hu, M., Yu, H., Liu, C., Chen, Z.: Design and experiment of a direct-drive wave energy converter using outer-PM linear tubular generator. IET Renewable Power Gener. 11(3), 353–360 (2017)
8. Zhang, J., Yu, H., Chen, M.: Direct-drive wave energy conversion with linear generator: A review of research status and challenges. IET Renewable Power Gener. (2022)
9. Almoraya, A.A., Baker, N.J., Smith, K.J., Raihan, M.A.H.: Design and analysis of a flux-concentrated linear vernier hybrid machine with consequent poles. IEEE Trans. Ind. Appl. 55(5), 4595–4604 (2019)
10. Faiz, J., Nematsaberi, A.: Linear electrical generator topologies for direct-drive marine wave energy conversion-an overview. IET Renewable Power Gener. 11(9), 1163–1176 (2017)
11. Shi, C., Qu, R., Gao, Y., Li, D., Jing, L., Zhou, Y.: Design and analysis of an interior permanent magnet linear vernier machine. IEEE Trans. Magn. 54(11), 1–5 (2018)
12. Liu, C., Zhu, H., Dong, R.: Linear magnetic gear with HTS bulks for wave energy conversion. IET Renewable Power Gener. 13(13), 2430–2434 (2019a)
13. Du, Y., Cheng, M., Chau, K.T., Liu, X., Xiao, F., Zhao, W.: Linear primary permanent magnet vernier machine for wave energy conversion. IET Electr. Power Appl. 9(3), 203–212 (2015)
14. Du, Y., Cheng, M., Chau, K.T., Liu, X., Xiao, F., Zhao, W., Shi, K., Mo, L.: Comparison of linear primary permanent magnet vernier machine and linear vernier hybrid machine. IEEE Trans. Magn. 50(11), 1–4 (2014)
15. Nematsaberi, A., Faiz, J.: A novel linear stator-pm vernier machine with spoke-type magnets. IEEE Trans. Magn. 54(11), 1–5 (2018)
16. Khaliq, S., Kwon, B.-I.: Design and analysis of a dual-stator spoke-type linear vernier machine for wave energy extraction. J. Electr. Eng. Technol. 11(6), 1700–1706 (2016)

17. Baloch, N., Khaliq, S., Kwon, B.-I.: HTS dual-stator spoke-type linear vernier machine for leakage flux reduction. IEEE Trans. Magn. 53(11), 1–4 (2017)
18. Liu, Y., Zhu, Z.-Q., Gan, C., Brockway, S., Hilton, C.: Comparison of optimal slot/pole number combinations in fractional slot permanent magnet synchronous machines having similar slot and pole numbers. J. Eng. 2019(17), 4585–4589 (2019b)
19. Hyoseok, S., Niguchi, N., Hirata, K.: Characteristic analysis of surface permanent-magnet vernier motor according to pole ratio and winding pole number. IEEE Trans. Magn. 53(11), 1–4 (2017)
20. Tlali, P.M., Wang, R.-J., Gerber, S., Botha, C.D., Kamper, M.J.: Design and performance comparison of vernier and conventional PM synchronous wind generators. IEEE Trans. Ind. Appl. 56(3), 2570–2579 (2020)
21. Wang, S., Zhao, W., Ji, J., Xu, L., Zheng, J.: Magnetic gear ratio effects on performances of linear primary permanent magnet vernier motor. IEEE Trans. Appl. Supercond. 26(7), 1–5 (2016)
22. Kolios, A., Di Maio, L.F., Wang, L., Cui, L., Sheng, Q.: Reliability assessment of point-absorber wave energy converters. Ocean Eng. 163, 40–50 (2018)
23. Li, L., Gao, Z., Yuan, Z.-M.: On the sensitivity and uncertainty of wave energy conversion with an artificial neural-network-based controller. Ocean Eng. 183, 282–293 (2019)
24. Wei, L., Nakamura, T.: A novel dual-stator hybrid excited permanent magnet vernier machine with halbach-array PMs. IEEE Trans. Magn. 57(2), 1–5 (2020)
25. Kang, M., Xu, L., Ji, J., Zhu, X.: Design and analysis of a high torque density hybrid permanent magnet excited vernier machine. Energies 15(5), 1723 (2022)
26. Kim, B., Lipo, T.A.: Operation and design principles of a PM vernier motor. In: Proceedings of 2013 IEEE Energy Conversion Congress and Exposition, pp. 5034–5041. IEEE, Piscataway, NJ (2013)
27. Heller, B., Hamata, V.: Harmonic Field Effects in Induction Machines. Elsevier Science & Technology, Amsterdam (1977).
28. Asef, P., Perpina, R.B., Barzegaran, M.: Global sizing optimisation using dual-level response surface method based on mixed-resolution central composite design for permanent magnet synchronous generators. IET Electr. Power Appl. 12(5), 684–692 (2018)
29. Asef, P., Perpina, R.B., Barzegaran, M.R., Lapthorn, A., Mewes, D.: Multiobjective design optimization using dual-level response surface methodology and booth's algorithm for permanent magnet synchronous generators. IEEE Trans. Energy Convers. 33(2), 652–659 (2017)

How to cite this article: Jafari, R., Asef, P., Sarhadi, P., Pei, X.: Optimal gear ratio selection of linear primary permanent magnet vernier machines for wave energy applications. IET Renew. Power Gener. 1–16 (2023). https://doi.org/10.1049/rpg2.12886